Transformation of Pan-STARRS1 *gri* to Stetson BVRI magnitudes. Photometry of small bodies observations.

A. Kostov & T. Bonev
Institute of Astronomy and NAO, Bulgarian Academy of Sciences, BG-1784, Sofia
`akostov@astro.bas.bg`

Abstract. The UBVRI broad band photometric system is widely used in CCD astronomy. There are a lot of sets of standard stars for this photometric system, the Landolt's and Stetson's catalogues being the most precise and reliable. Another photometric system, recently considerably spread in CCD observations is *ugriz*, which originates from the Sloan Digital Sky Survey (SDSS) and has now many variations based on its 5 broad-band filters. One of the photometric systems based on it is The Panoramic Survey Telescope and Rapid Response System (Pan-STARRS). In this paper we compare the BVRI magnitudes in the Stetson catalogue of standard stars with the magnitudes of the corresponding stars in the Pan-STARRS1 (PS1) *grizy* catalogue. Transformations between these two systems are presented and discussed. An algorithm for data reduction and calibration is developed and its functionality is demonstrated in the magnitude determination of an asteroid.

Key words: Surveys – Catalogs – Techniques: photometric – Comets: general – Minor planets, asteroids: general

Introduction

One peculiarity of the observations of moving objects is the constantly changing observed field. Every comet or asteroid has unique proper motion, in general absolutely different from the celestial one. In case of fast moving objects, there can be several different observed fields in the same night. Due to that feature, calibration of instrumental magnitudes with photometric standard stars is more difficult in comparison to observations of fixed star fields, and establishing a good set of secondary photometric standards is virtually impossible. It gets evident that in the case of small bodies photometry one needs an all-sky spread standard stars in the BVRI photometric system. Hence the main goal of this work is to obtain reliable relation between an all-sky catalogue PS1 and Stetson BVRI standard stars catalogue (**Stetson Homogeneous photometry database**[1]).

Before the release of PS1 we used to calibrate our photometry with the only suitable broad-band all-sky catalogue - the USNO B1.0 (Monet et al.

---

[1] `http://www.cadc-ccda.hia-iha.nrc-cnrc.gc.ca/en/community/STETSON/standards/`

2003). Covering the B and R passbands this catalogue shows excellent sky coverage and astrometric precision. Unfortunately USNO B1.0 is characterized by a poor photometric accuracy. Nevertheless we used USNO B1.0 following Kidger (2003). We did some attempts to improve our data calibration by using additional re-calibrations of USNO B1.0 photometry, as suggested by Madsen and Gaensler (2013). The connections between SDSS photometric systems and BVRI (Jordi et al. 2006), were noted but could not be used, because of the insufficient coverage of the sky. With the release of PS1, this problem is solved, and this motivated us to obtain a relation between PS1 and Stetson's BVRI photometric standards.

1   Choice of the photometric system

One of the cornerstones in astronomy is the establishment of reliable celestial objects magnitudes. Selection of a proper photometric system with a suitable set of primary standards is the first, and most important step of obtaining accurate photometric results. There is a large number of photometric systems covering different spectral ranges. One of the most widely used and well established broad-band photometric system is the Johnson-Cousins UBV Kron-Cousins RI (UBVRI). Being one of the first photometric systems, UBVRI underwent a long evolution (Bessell 2005). Nowadays the most used set of filters representing this system is Johnson/Bessell (Bessell,1990). Further in this work we will omit the U band filter for two main reasons: first, there is a lack of data in Stetson's catalogue for U, and second, with very rare exceptions, our observations of small bodies practically did not include the U band.

As was stated above the standardization of stellar photometry presented in this investigation is based on the use of the Stetson's catalogue of CCD standard stars (Stetson, 2000). Initially based on the Landolt (1992) UBVRI photometry, today Stetson's catalogue comprises a large set of fields covering wide range of declinations. Observations are multy-epoch, extended down to magnitudes fainter than 20 mag. The stellar photometry is homogeneous, precise and regularly updated.

In the last two decades several digital sky surveys use one new photometric system, which may become a new standard in photometric observations. This is the *ugriz* photometric system of the SDSS and it's variations (Fukugita et al. 1996). Pan-STARRS1 survey (Chambers et al 2016) is build on observations obtained by *grizyw* photometric system, and since 12 December 2016 the **Pan-STARRS1 Catalogue Search**[2] is public. The survey is multy-epoch, it covers the entire North sky, extends to declinations $-30°$, contains wide range of magnitudes with milimagnitude accuracy (Tonry et al. 2012; Magnier et al. 2016a), and give us the opportunity to use it as a secondary standard catalogue. Further in this work we will use only the first half of the entire PS1 photometric system - *gri*. The *zyw* does not correspond to the aim of our task, and as such will be omitted in the transformation equations.

---

[2] `http://archive.stsci.edu/panstarrs/search.php`

The transmissions of the BVRI (Bessell,1990) and the *gri* filters[3] (Tonry et al., 2012) are presented in Fig.1[4]. The profiles of the filters and the covered spectral ranges are quite different, and there is no simple connection $V = f(g)$, $R = f(r)$ or $I = f(i)$. Due to that we decided to compare both photometric systems in more details using colours instead of magnitudes in the transformation equations.
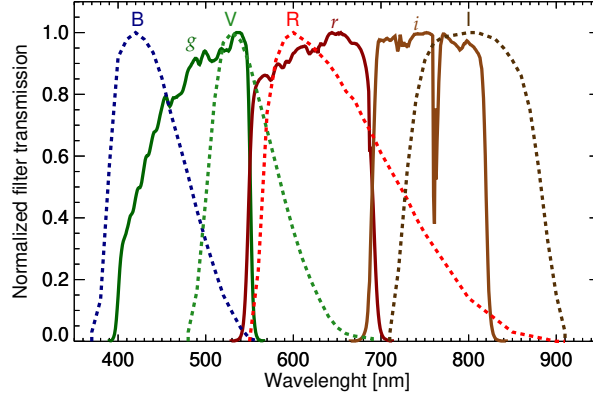

Fig. 1. Comparison of Johnson/Bessell BVRI and Pan-STARRS1 *gri* filters transmission curves.

---

[3] http://iopscience.iop.org/0004-637X/750/2/99/suppdata/apj425122t3_mrt.txt

[4] Further in this work we will use the same colours of the filters as in Fig.1 for representing the features connected to BVRI or *gri*

2   Catalogues Data

For the purposes of our work 73 fields from Stetson's database[1] were selected. In order to obtain relation between both catalogues, only fields for which BVRI photometry is available were used. The sample covers declinations between $-30°$ and $+85°$ and includes as many different sky patches as possible (Fig.2).
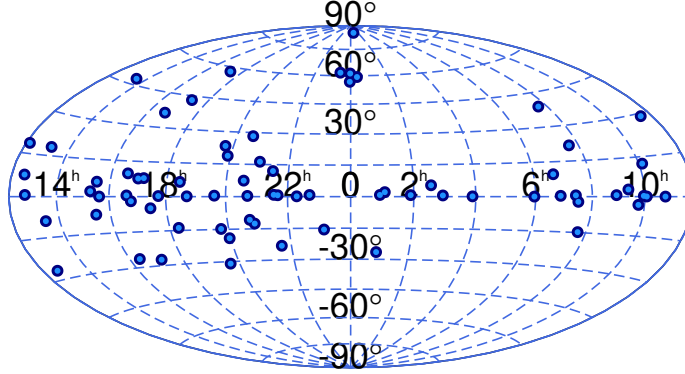

Fig. 2. Distribution of the used fields across the celestial sphere. The coordinate system of the chart is equatorial.

That initial sample contains 33026 Stetson's standard stars which were cross-identified with PS1 observations. The PS1 catalogue search tool[2] (Flewelling et al., 2016) provide a lot of useful options, such as possibility to upload data file with coordinates and simultaneously identify group of objects (for example all stars from a given observed field can be identified in one run). The image quality of PS1 survey is evaluated by Magnier et al. (2016c) with a median $FWHM = [1.31(g), 1.19(r), 1.11(i)]''$. The PS1 nominal plate scale of $0.258''$ per pixel (Waters et al. 2016) corresponds to a median PSF of a star about 5 pixels. The astrometric accuracy of the PS1 is $0.022''$ for the right ascension (α) and $0.023''$ for the declination (δ) (Magnier et al., 2016c). Although Stetson has not provided individual astrometric errors for the positions of the stars, in his database[1] the coordinates of the stars are given with accuracy of 0.01^s i.e. $0.15''$ for α and $0.1''$ for δ. In order to produce a homogeneous star list, and to avoid spurious cross-identifications, we used to split the selection process in 3 steps (depending on the search radius used with the PS1 catalogue search tool[2]) as follows:

- **step1**: search all 33026 Stetson's stars in PS1 catalogue within a search radius $R = 3 \times \sqrt{(0.15^2 + 0.1^2)} = 0.541''$. This yields 24903 cross-identifications, 75.4% of the initial sample.

After this first step a manual check of random selected not-cross-identified objects was performed. Stars with different magnitudes were checked in the **Image Cutout Server**[5] tool of the PS1 archive. This test shows that a significant number of good defined stars, without neighbours or near arte-facts, do not match the first criterion. The possible reasons for that pitfall are explained in **PanSTARRS Search Help**[6] under the description of the **Radius**: *'You should be careful about giving too restrictive a search radius since (for some missions) the coordinates of the object were given by the Guest Observer, and may not reflect the precise pointing of the instrument at the time of the observation'*. To extend our sample we applied the next 2 steps:

- **step2**: search all not-cross-identified 8123 stars within $R = 0.655''$. In order to account for possible shifts of stars positions, related to the quality of the image, we extended the search aperture to the median $FWHM$ of PS1. This second search adds more tan 6102 stars to the list of cross-identified stars.

- **step3**: search all remaining 2021 stars with $R = 2.62''$, i.e $2 \times FWHM(g)$. This generous search radius gives 2005 new matches. To prevent the sample from nonstar identifications (see Fig. 3 in Magnier et al. 2016b) we decided to use only these with angular separation $\rho \leq 1.0''$, which are 1768 stars.
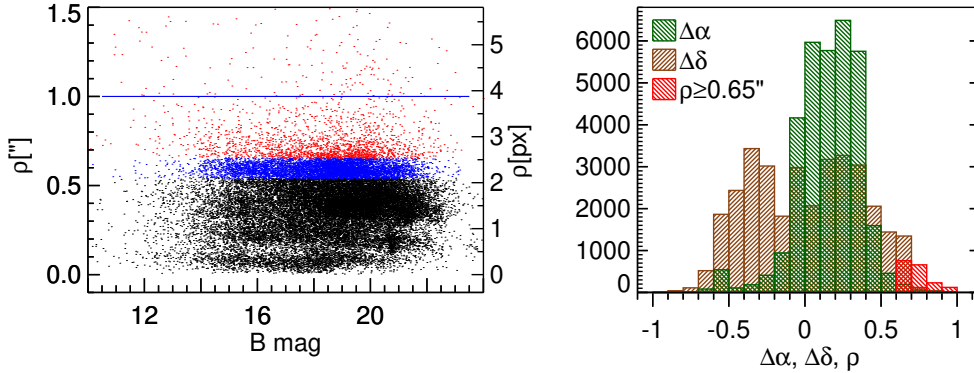

Fig. 3. Angular separations (left) and differences in α, δ (right) for 32773 cross-identified stars.

The final cross-identification list contains 32773 stars, which is 99.2% of the initial Stetson's data. The angular distance between the Stetson's stars and their PS1 counterparts is a good measure for the quality of the cross-identification. Fig.3 shows the distribution of these angular distances.

_____

[5] http://ps1images.stsci.edu/cgi-bin/ps1cutouts
[6] http://archive.stsci.edu/panstarrs/help/search_help.html

In the left panel of Fig.3 the left ordinate is in arcseconds, and the right one shows the corresponding distances in pixels. The black dots are the stars with $\rho \leq 0.541''$, the blue dots are the stars within $\rho = [0.541, 0.655]''$, and the red dots are the stars within $\rho = [0.655, 2.62]''$, the upper limit of the latter being outside of the ordinate range. Below the blue line $(1.0'')$ are all stars which passed the astrometric criteria. For them, in the right panel of this figure, the distributions of the differences in α, δ are shown. In this histogram plot is also shown the distribution of ρ for the set of 1768 stars, selected by using the selection criterion described in **step3**. As seen, the number of stars drops rapidly, and for $\rho > 1.0''$ the number of omitted stars is as low as 237.

After finishing the astrometric cross-identifications, we set 3 more conditions, depending on photometric data of the selected stars:

- All stars must have Stetson BVRI and PS1 *gri* magnitudes. This criterion removes 612 stars from the list.

- According to Stetson (2000) his database[1] satisfies the following criterion: *'at least five independent observations under photometric conditions and standard errors of the mean magnitude smaller than 0.02 mag'*. We applied the second part of this requirement to the cross-identified PS1 stars, i.e. we removed from the final list selected set all stars having photometry errors greater than 0.02 magnitudes. This criterion removes 8198 stars.

- All stars are restricted to magnitude < 19 mag.(see the note at the end of section 3 for more detailed explanation of this criterion). Application of this criterion removes 14971 stars from the list.

Note that all three photometric criteria were applied simultaneously, and the final amount of removed stars from the cross-identification list is 17699. Because some of the stars met more than one criterion, the reduction of the list is not a simple sum of the removals of each criterion. The final list of stars which we used to derive the colour transformations between PS1 *gri* and Stetson's BVRI catalogue was reduced to N = 15074. These standard stars are distributed in 68 Stetson's fields. Table 1 contains the names of the fields (column 1) as given in the database[1], the central coordinates of the fields for epoch (2000.0) (columns 2-7) and the number of stars for each particular field (column 8) used to derive the colour transformations.

Table 1. Stetson standard fields used for comparison with PS1 catalogue

Field	RA	DEC	N	Field	RA	DEC	N	Field	RA	DEC	N
NGC6809	19 40.0	-30 57.7	130	L98	06 52.0	-00 20.6	1502	UGC10743	17 11.3	+07 56.0	203
Barnard59	17 11.7	-27 24.9	61	L101	09 57.3	-00 17.3	337	NGC2264	06 41.1	+09 38.3	74
NGC4590	12 39.5	-26 44.6	31	L109	17 44.7	-00 15.4	198	PG1633	16 35.5	+09 47.0	268
NGC288	00 52.5	-26 27.7	173	PG2213	22 17.4	-00 08.8	111	NGC7078	21 29.6	+11 59.3	113
NGC6121	16 23.3	-26 25.3	166	Pal3	10 04.2	-00 03.0	43	LeoI	10 08.3	+12 23.1	154
NGC7099	21 40.3	-23 10.5	166	PG1047	10 50.0	-00 01.0	18	NGC7006	21 01.4	+16 17.1	188
133P	19 57.5	-19 07.7	37	L107	15 38.5	+00 02.9	650	NGC5024	13 12.9	+18 10.2	207
NGC7492	23 08.1	-15 36.7	29	L95	03 53.6	+00 07.3	225	NGC4147	12 10.2	+18 31.4	77
NGC2437	07 41.8	-14 48.9	246	L110	18 42.8	+00 08.3	322	NGC6838	19 53.9	+18 46.7	35
NGC6822	19 44.7	-14 46.8	311	L112	20 42.6	+00 19.7	37	NGC2420	07 38.4	+21 34.4	145
Messier16	18 18.6	-13 50.9	246	L111	19 37.7	+00 27.0	77	NGC6823	19 43.2	+23 18.0	37
NGC6981	20 53.5	-12 32.2	48	L113	21 41.1	+00 39.2	672	NGC6940	20 34.6	+28 16.1	127
MarkA	20 44.7	-10 45.9	822	L114	22 41.9	+00 46.8	2	Pal4	11 29.3	+28 58.4	8
PG1323	13 26.2	-08 58.4	528	L92	00 55.5	+00 47.7	221	NGC6205	16 41.7	+36 27.6	187
PG1525	15 28.2	-07 15.7	384	IC1613	01 04.8	+02 07.1	86	NGC2419	07 37.9	+38 54.5	127
NGC6366	17 27.4	-05 01.2	64	NGC5904	15 18.2	+02 08.1	1105	NGC6341	17 17.1	+43 08.2	585
PG0942	09 45.2	-03 08.5	22	PG0918	09 21.7	+02 46.5	104	NGC7789	23 57.4	+56 42.5	19
Ru152	07 29.8	-02 10.3	137	PG0231	02 33.7	+05 18.7	26	Draco	17 19.4	+57 55.5	51
NGC6218	16 47.2	-01 56.9	172	PG1528	15 30.8	+06 01.3	19	IC10	00 20.4	+59 17.6	48
NGC7089	21 33.4	-00 50.7	437	NGC6633	18 27.3	+06 31.8	46	NGC7790	23 58.4	+61 13.0	235
L104	12 42.1	-00 35.6	298	NGC6934	20 34.2	+07 24.2	94	NGC7654	23 24.9	+61 38.9	116
Ru149	07 24.3	-00 32.9	1429	NGC4526	12 34.1	+07 42.0	6	NGC188	00 47.5	+85 16.2	172
L108	16 37.9	-00 30.1	9	PG1657	16 59.6	+07 42.4	51				

3 Transformation equations

The comparison between PS1 *gri* and Stetson's BVRI magnitudes could be described with the following seven relations:

$$B-g = C_0+C_1\times(g-r) \qquad B-g = D_0+D_1\times(g-r)+D_2\times(g-r)^2 \tag{1}$$

$$V-g = C_0+C_1\times(g-r) \qquad V-g = D_0+D_1\times(g-r)+D_2\times(g-r)^2 \tag{2}$$

$$V-r = C_0+C_1\times(g-r) \qquad V-r = D_0+D_1\times(g-r)+D_2\times(g-r)^2 \tag{3}$$

$$R-r = C_0+C_1\times(g-r) \qquad R-r = D_0+D_1\times(g-r)+D_2\times(g-r)^2 \tag{4}$$

$$I-i = C_0+C_1\times(g-r) \qquad I-i = D_0+D_1\times(g-r)+D_2\times(g-r)^2 \tag{5}$$

$$R-r = C_0+C_1\times(r-i) \qquad R-r = D_0+D_1\times(r-i)+D_2\times(r-i)^2 \tag{6}$$

$$I-i = C_0+C_1\times(r-i) \qquad I-i = D_0+D_1\times(r-i)+D_2\times(r-i)^2 \tag{7}$$

where (C_i) and (D_i) are the coefficients in the first and second order approximations, respectively. The resulting coefficients derived from fits to the data are summarised in Table 2. Here the first and the second columns contains the coefficients of the linear fit, followed by the standard deviation of the fit, σ. The columns 4-6 contain the coefficients of the quadratic fit, and in column 7 is the standard deviation of this fit, σ_2. The uncertainties

are placed under the coefficients. In most of the cases the standard deviation of the linear fit is sufficiently small, and the coefficients (C_0, C_1), derived from the first order link between both photometric systems can be used with confidence. We observe a slight deviation from the liner fits around the boundaries of the used colours. The linear fit is correct for colours $(g-r)$ in the range [-0.5, 1.5], and for $(r-i)$ in the range [-0.4, 1.0] (see Fig. 4 and Fig. 5), i.e. practically for more than 80% of the colour range, excluding stars with extremely red colour indices.

Table 2. Transformation coefficients derived from the linear (C_i) and second order (D_i) fits of the data described by equations (1)÷(7)

C_0	C_1	σ	D_0	D_1	D_2	σ_2
			$B - g = f(g - r)$			
0.194	0.561	0.056	0.199	0.540	0.016	0.056
(±0.001)	(±0.002)		(±0.001)	(±0.004)	(±0.003)	
			$V - g = f(g - r)$			
-0.017	-0.508	0.032	-0.020	-0.498	-0.008	0.032
(±0.001)	(±0.001)		(±0.001)	(±0.002)	(±0.002)	
			$V - r = f(g - r)$			
-0.017	0.492	0.032	-0.020	0.502	-0.008	0.032
(±0.001)	(±0.001)		(±0.001)	(±0.002)	(±0.002)	
			$R - r = f(g - r)$			
-0.142	-0.166	0.042	-0.163	-0.086	-0.061	0.041
(±0.001)	(±0.001)		(±0.001)	(±0.003)	(±0.002)	
			$R - r = f(r - i)$			
-0.166	-0.275	0.038	-0.172	-0.221	-0.081	0.036
(±0.000)	(±0.002)		(±0.000)	(±0.002)	(±0.002)	
			$I - i = f(g - r)$			
-0.376	-0.167	0.054	-0.387	-0.123	-0.034	0.054
(±0.001)	(±0.001)		(±0.001)	(±0.004)	(±0.003)	
			$I - i = f(r - i)$			
-0.416	-0.214	0.061	-0.433	-0.040	-0.263	0.048
(±0.001)	(±0.003)		(±0.001)	(±0.003)	(±0.003)	

In most of the cases the coefficients of the quadratic term in the second order fits have values lower than the standard deviations of the fits (both, first and second order). Here we have two exceptions: the $(r - i)$ colour equations (6)÷(7) have significantly higher quadratic terms, and in this cases, the quadratic fits should be used for red stars, where these distributions are described better in comparison to the linear fit (see Fig. 4, Fig. 5). In general, quadratic solutions should be used for the regions close to the boundaries of the used colours.

The results are in very good agreement with Tonry et al. (2012) who studied equations (1)÷(5), using synthetic magnitudes with colours ranging

from the colour of the Sun to that of Vega, i.e. their transformations don't cover the range $(g - r) = [1.5, 2.5]$, where we notice deviations from the linear fits.
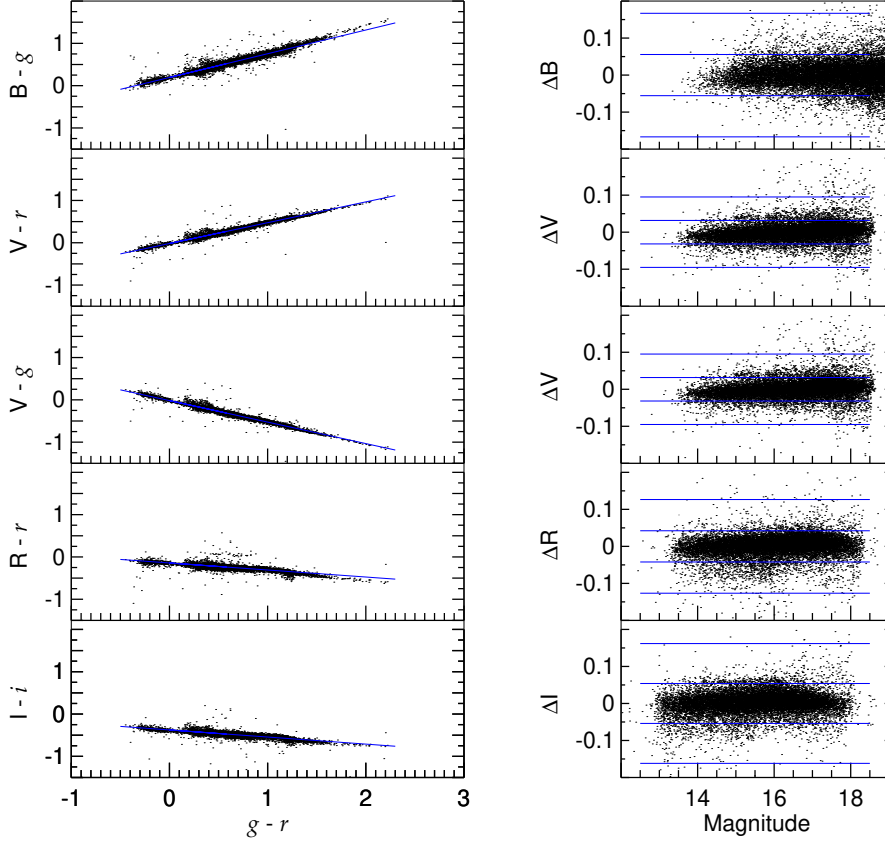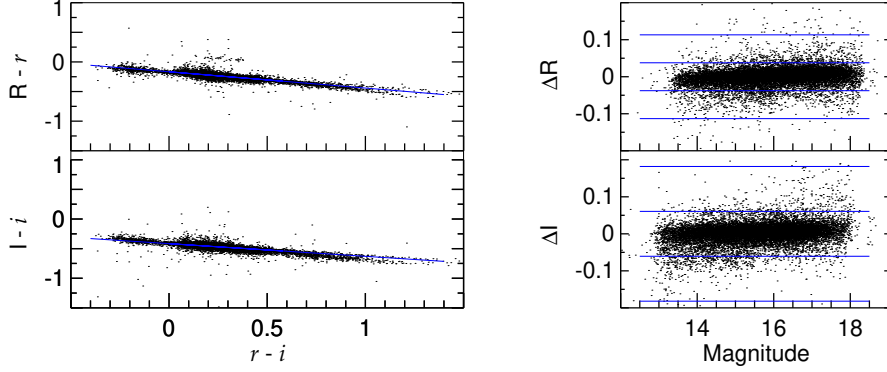

Fig. 4. Left: Transformations between Stetson's and PS1 standard stars magnitudes as a function of $(g - r)$ colour indices. Right: Corresponding differences between transformed and Stetson's magnitudes versus magnitude.

Having the coefficients in the transformation equations we can visualize the results by plotting them against the corresponding colour. The transformations were divided into 2 groups, depending on the colour: $(g - r)$ colour group (equations (1)÷(5)), which are presented in Fig. 4, and $(r - i)$ colour group (equations (6)÷(7)), which are presented in Fig. 5. On these similar figures on the left side are shown colour-colour plots for 15074 cross-identified stars. Here the corresponding linear fits are plotted with blue lines. The right columns of these figures contain the deviations of the calcu-

lated values from the Stetson's catalogue magnitudes presented as function of magnitude, $\Delta m = m_{catalogue} - m_{calculated}$.

The derived differences don't show significant bias from the zero slope. Only in the case of V filter equations, (2) and (3), an increase of the deviations is visible, but $\sim 99\%$ of all ΔV values are inside of the $\pm 3\sigma$ range. Here the blue lines represent $\pm\sigma$ and $\pm 3\sigma$ of the corresponding transformation fit. The majority of the differences Δm are within $\pm 3\sigma$ of the fit.

Fig. 5. Left: Transformations between Stetson's and PS1 standard stars magnitudes as a function of $(r - i)$ colour indices. Right: Corresponding differences between transformed and Stetson's magnitudes versus magnitude.

Histogram distributions of the differences, Δm are shown in Fig. 6. Each histogram plot from left to right represents the distribution of Δm derived from equations (1)÷(7). For all transformation equations up to $\sim 86\%$ of the stars differ from the catalogue magnitudes within $\pm\sigma$, and up to $\sim 98\%$ of the stars deviate from their catalogue magnitudes within $\pm 3\sigma$. Here σ is the standard deviation of the fits presented in the left panels of Fig. 4 and Fig. 5 (see also Table 2, column 3, σ). Each of the histograms was fitted with a Gaussian function. The derived distributions are highly symmetrical around the zero point, close to Gaussian functions, with exception of their higher wings and maxima. There is a slight bias of the wings in negative direction for all distributions, pointing that the calculated magnitudes of stars with greater errors are systematically greater (fainter) compared to the catalogue's. The distributions are characterized by similar maxima - all around 3000, with exception of $\Delta B(g - r)$ (i.e. equation (1)), which has a lower maximum (2033) and wider wings (note the more 'noisier' scatter of the data in the top right plot of Fig. 4). The lower right plot in Fig. 6 shows the Gaussian fits to each of the 7 histograms, normalized to their maxima. Here only the blue Gaussian $(\Delta B(g - r))$ differs from all other, being broader. We do not observe any humps or tails in the distributions, which is an indication of coherence and homogeneity between the compared photometric systems.
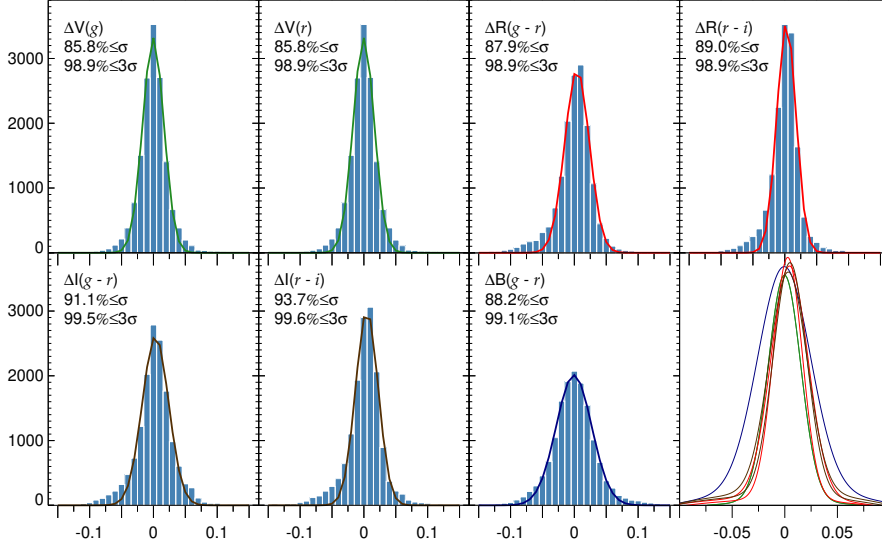
Fig. 6. Distributions of the differences "calculated values - Stetson's magnitudes", $\Delta m = m_{catalogue} - m_{calculated}$ (corresponds to the data presented in the right panels of Fig. 4 and Fig. 5).

Note: There were 3 photometric limits set to the cross-identified stars. The limiting magnitude is the most questionable one. To check the selection of a reasonable limiting magnitude we calculated the differences between the catalogue magnitudes and the results of the transformation equations, and analysed their dependence on the number of stars, which results from the magnitude limit. As a measure of the quality of the transformation we used the standard deviation of the linear fit, σ. Fig. 7 presents the standard deviations of linear and quadratic fits for each 7 transformation equations, for 8 different limiting magnitudes, ranging from 16 mag to 23 mag. Restricting the sample to brighter stars, or extending it to the maximum of the magnitude range, raises the errors and noise in the resulting transformations. Minimum of the 1-sigma uncertainties is visible in the magnitude range 18-19 mag. Limiting magnitude of 19 mag gives more populated and thus more representative sample of stars, and therefore it was selected as one of the photometric criteria.
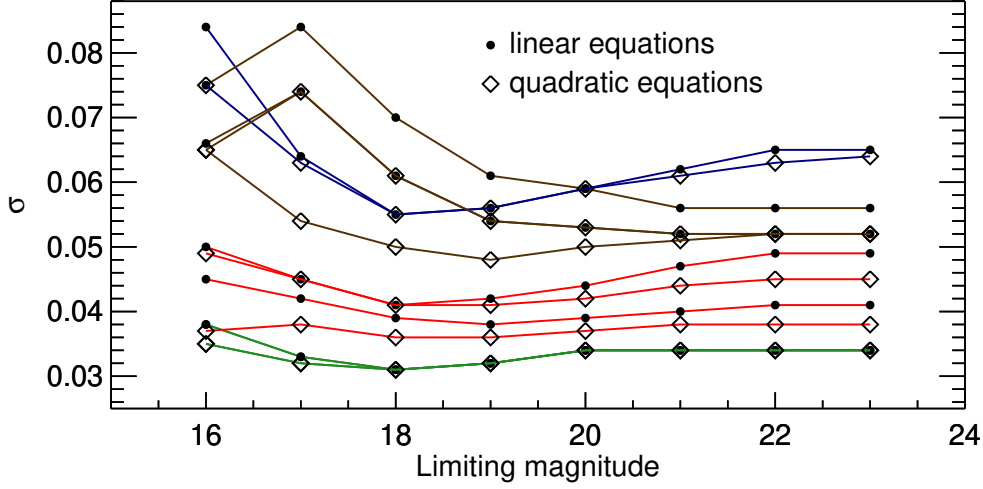
Fig. 7. Standard deviations, σ of the fits, described by the transformation equations (1)÷(7) depending on the limiting magnitude, greater and smaller than 19 mag (photometry criterion 3).

4 Verification with original observations

The equations, presented in the previous section, show the relation between two standard stars catalogues, PS1 and Stetson. In order to test the reliability of these catalogue-to-catalogue relations we observed three of the Stetson's fields listed in Table 1: L107, NGC5904 and NGC6341. The observations were obtained with the Schmidt telescope of the National astronomical observatory Rozhen, Bulgaria[7].

   The standard procedures of dark subtraction, and flat field divisions were applied to the observational data. After that the initial astrometric solutions for all images were found and all point sources were detected. For each object two sets of coordinates were derived - (X, Y) and (α, δ). All objects were searched (trough their α, δ coordinates) in the PS1 catalogue search tool[2], and a cross-identification list for each image was made. Aperture photometry of all objects was performed. Then the transformations (1)÷(7), with their coefficients (Table 2), were applied to the PS1 catalogue magnitudes gri, to obtain the transformed magnitudes m' - $B'V'R'I'$ (the prime-quantities were introduced as an intermediate designation, preserving BVRI for the final result). The relation between instrumental magnitudes and those calculated by using the transformations (1)÷(7) can be expressed by a simple linear relation:

$$m_{inst} = Z + S \times m', \tag{8}$$

---

[7] http://nao-rozhen.org/telescopes/fr17.html

where Z is the zero point, and S is the slope. Applying a linear fit to the data, the slope and zero point were derived. The results of the fitting procedure are shown in Fig. 8, Fig. 9 and Fig. 10. The left column of plots in these figures represents the instrumental magnitudes against the transformed $B'V'R'I'$ magnitudes. These fits are plotted in two colours: blue lines represent $(g-r)$ colour group (equations (1)÷(5)), and the members of the $(r-i)$ colour group are red (equations (6) and (7)). The connections between instrumental and $B'V'R'I'$ magnitudes are well described by linear fits with slopes close to 1.0 and zero points in the interval [-6.92,-5.94]. The photometric coefficients for all test images are presented in tables 3, 4, and 5. In these tables the four rows contain N - the number of stars used to estimate the zero point and the slope, S - the slope, Z - the photometric zero point for each image, and σ - the standard deviation of the linear fit. The numbers under the values of S and Z are their 1-sigma uncertainty estimates.

With the derived zero point and slope, the standard magnitude of any object can be calculated:

$$m_{calculated} = (m_{inst} - Z)/S \qquad (9)$$

In this test we consider the Stetson's standards as 'unknown' objects. The instrumental magnitudes of these 'unknown' objects are used now together with the derived photometric coefficients, Z and S, to obtain their calculated magnitudes, ($m_{calculated}$). Comparing them to the catalogue magnitudes for each 'unknown' Stetson standard we can verify the reliability of the transformation equations (1)÷(7). In the right plots of figures 8, 9, and 10 the deviations between the catalogue and the calculated Stetson's magnitudes $\Delta m = m_{catalogue} - m_{calculated}$ are shown. Here the blue lines represent $\pm\sigma$ and $\pm 3\sigma$ of the transformation plots. Symbol n in the panels stays for the numbers of the checked Stetson standards. Deviation's scatter grows up in the direction of fainter magnitudes, where the instrumental values are derived with higher errors. Nevertheless the majority of the differences are close to the zero line, and within the 3σ limits of the fits, indicating that the transformations are coherent. The deviations of the magnitudes for NGC6341 are shifted from the zero line in positive direction, indicating overestimation of the instrumental magnitudes. The bias is around 1-sigma and rises significantly for fainter stars. One possible explanation of this result is the very low metallicity of the NGC6341 (M92) [Fe/H] = -2.31 (Harris 1996)[8]. The metal-poor Globular Clusters, like NGC6341, carry Population II stars, and this can affect the transformation equations, as assumed by Jordi et al. (2006). For the other two Stetson's fields, as for the general sample, we do not observe any effects of the metallicity on the transformation equations.
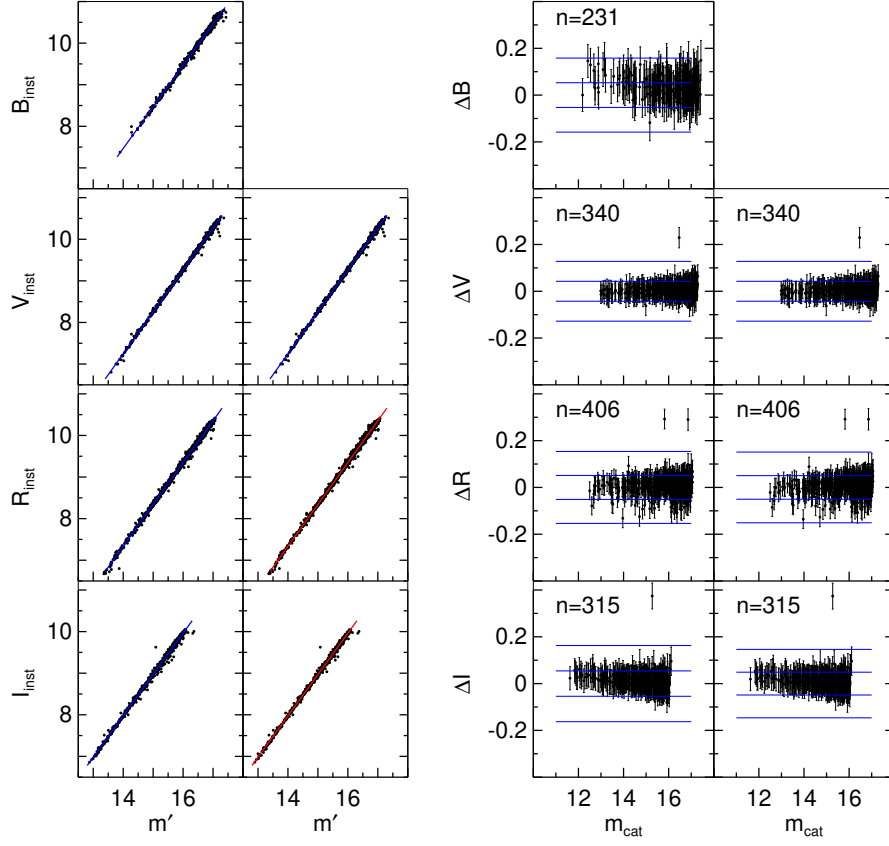
---

[8] http://physwww.physics.mcmaster.ca/~harris/mwgc.dat

Fig. 8. Left: Instrumental magnitudes compared to transformed $B'V'R'I'$ magnitudes for all 7 equations. Right: Deviations of the calculated Stetson's magnitudes relative to their catalogue values $\Delta m = m_{catalogue} - m_{calculated}$. Stetson's field L107

Table 3. Photometric coefficients for L107

	B	V		R		I	
N	454	677		903		696	
S	0.997	1.008	1.008	1.006	1.008	0.994	0.995
	(±0.003)	(±0.002)	(±0.002)	(±0.002)	(±0.002)	(±0.003)	(±0.002)
Z	-6.50	-6.86	-6.86	-6.75	-6.78	-5.94	-5.95
	(±0.06)	(±0.03)	(±0.03)	(±0.03)	(±0.03)	(±0.04)	(±0.03)
σ	0.05	0.04	0.04	0.05	0.05	0.05	0.05
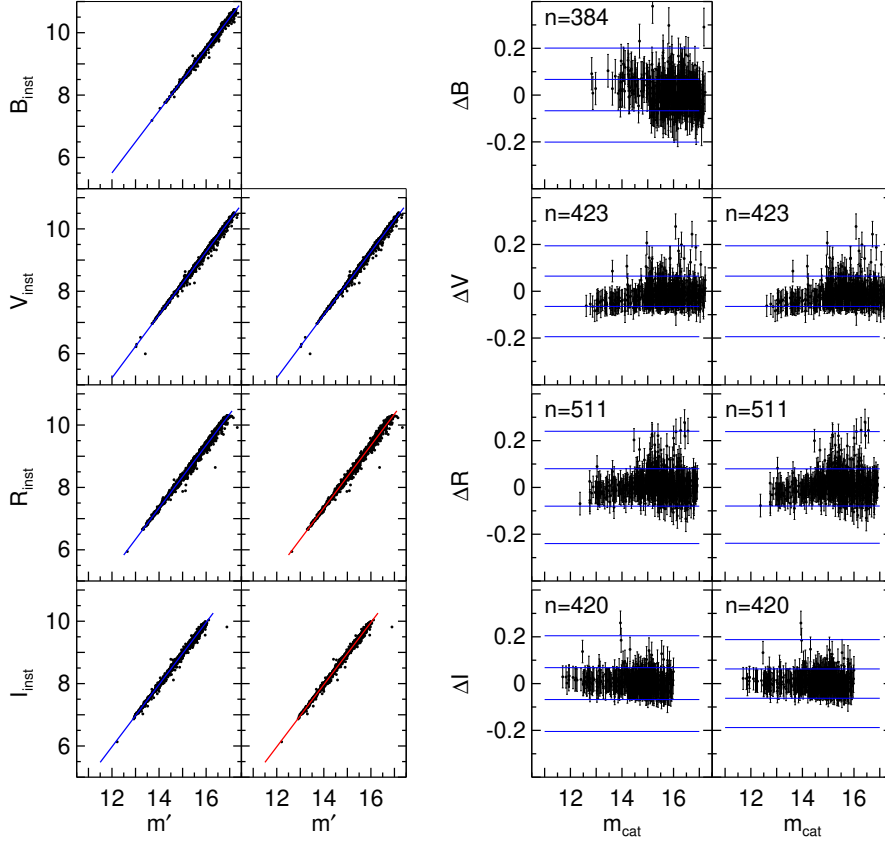
Fig. 9. Same as Fig. 8, but for Stetson's field NGC5904

Table 4. Photometric coefficients for NGC5904

	B	V		R		I	
N	787	1162		1574		1278	
S	0.993	1.010	1.010	1.004	1.007	0.997	1.000
	(±0.003)	(±0.002)	(±0.002)	(±0.002)	(±0.002)	(±0.002)	(±0.002)
Z	-6.42	-6.90	-6.90	-6.72	-6.76	-5.99	-6.03
	(±0.05)	(±0.04)	(±0.04)	(±0.04)	(±0.04)	(±0.04)	(±0.03)
σ	0.07	0.06	0.06	0.08	0.08	0.07	0.06

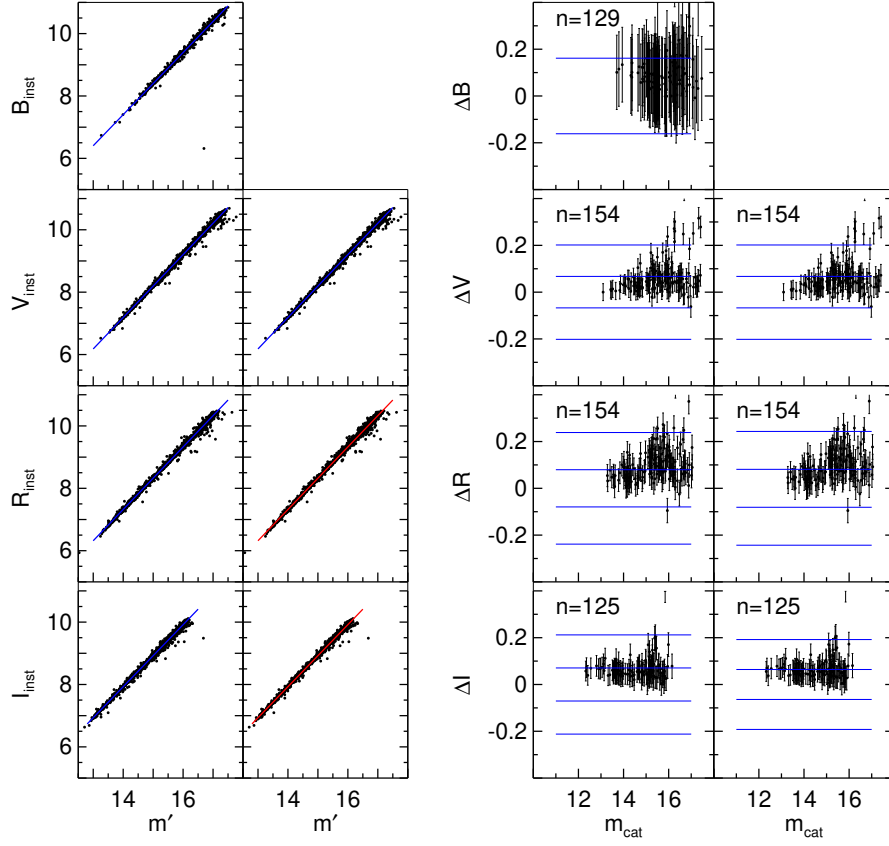**Fig. 10.** Same as Fig. 8, but for Stetson's field NGC6341

Table 5. Photometric coefficients for NGC6341

	B	V		R		I	
N	670	1615		1392		1496	
S	0.996	1.007	1.007	1.003	1.006	0.994	0.995
	(±0.007)	(±0.002)	(±0.002)	(±0.002)	(±0.002)	(±0.002)	(±0.002)
Z	-6.54	-6.92	-6.92	-6.72	-6.77	-5.99	-6.00
	(±0.12)	(±0.03)	(±0.03)	(±0.03)	(±0.03)	(±0.03)	(±0.03)
σ	0.16	0.07	0.07	0.08	0.08	0.07	0.06

5   Photometry of small bodies observations

Photometry of small bodies in the Solar System always faces the problem of finding reliable standards in the observed field. Usually in-field photometric standards are missing, and one way to obtain the magnitudes is to apply relative photometry. In this method it is essential to have significant number of stars in the observed field, which will be used as secondary standards. The problem with the so called 'secondary standards' is that they actually are not standard stars. Many of them suffer from numerous disadvantages: they are variable, they not stars, magnitudes are not accurate, etc. Hence their number in the process of calibration is so important. Using a large number of secondary standards can minimise the impact of biased instrumental magnitudes. Fortunately observations with a wide-field telescope system (field of view $> 1°$), offer thousands of stars with suitable S/N ratio in the field of every target. The significant number of stars which can be used as secondary standards makes the calibration of the instrumental magnitudes possible. As stated in the Introduction the most suitable source for a large number of stars homogeneously distributed all over the sky is PS1. The equations (1)÷(7), can be used to transform *gri* to BVRI, making the data compatible with any other observation obtained with or transformed to this standard system.

The procedure, that we followed to calibrate observations of small bodies, follow the steps of the verification of the transformation equations, described in the previous section. These steps are:

- Find initial astrometric solution of the observed field.
- Identify all point sources in the image and record their in-image position coordinates (X, Y), along with their celestial coordinates (α, δ).
- Use the PS1 catalogue search tool[2] to cross-identify all selected stars.
- Derive the instrumental magnitudes of all cross-identified stars.
- Use the transformation equations (1)÷(7) with their coefficients (Table 2) to transform all *gri* to $B'V'R'I'$ magnitudes.
- Derive the photometric coefficients, Z and S, of each image, comparing the instrumental magnitudes with $B'V'R'I'$ magnitudes.
- With the derived photometric zero point and slope calibrate the instrumental magnitudes of the observed object (comet or asteroid) to standard BVRI magnitude.

To optimise the procedure, and to provide robust transformations, it is advisable to set some criteria for sampling reasonable sets of stars, which will be used in deriving the transformation coefficients of the images. One possibility in this respect is to use the astrometric and photometric criteria, described in this paper, in order to minimise the instrumental magnitudes uncertainty caused by poor photometry/astrometry.

To give an example how the described algorithm works, we checked the BVRI images of NGC5904 for moving objects using the software package **ASTROMETRICA**[9] by Raab (2012). One of the detected objects was the main-belt asteroid 48220. Application of the procedure to that

---

[9] http://www.astrometrica.at/

object, with unknown photometric parameters, resulted in following calculated magnitudes: $B = 19.12 \pm 0.14$, $V = 18.29 \pm 0.08$, $R = 17.93 \pm 0.08$ and $I = 17.61 \pm 0.11$. The V magnitude is in good agreement with the ephemeris magnitude given by **HORIZONS**[10], the on-line Solar system data and ephemeris described by Giorgini et al. (1996). The derived colours of the asteroid are $B - V = 0.829 \pm 0.165$, $V - R = 0.364 \pm 0.109$ and $R - I = 0.317 \pm 0.131$. Within the limits of the photometric uncertainties, these colours resemble closely the colours of the Sun (Ramírez et al. 2012). This neutral reflectance is a typical property of carbonaceous bodies, which gives a reason to consider 48220 a member of the mostly populated taxonomic class of C-type asteroids.

6   Conclusions

In this paper we present relations between two standard star systems, namely Stetson's BVRI and Pan-STARRS1 *gri*, established by means of seven transformation equations. Using cross-identification, a set of 15074 stars form Stetson's database[1] and PS1 catalogue[2] was extracted and used to derive the transformation equations coefficients. Comparison of the derived coefficients and their uncertainties revealed that the linear fit gives reliable results. Verification tests were performed applying them to three Stetson's standard fields. The results of these tests confirmed the reliability of the transformation equations. There were several features (like the slight deviation from linearity for extremely red stars, or the influence of Population II stars on the results for NGC6341) that do not impact the final results, but can be subject of a future study, going into more details in that direction. The proposed procedure of relative photometry can be used for wide range of tasks (when standards do not exist in the observed field): observations of variable stars, exoplanets, optical transients etc. The relative photometry of small bodies observations using these transformations is a possible task, and this is the field where they will find wide and effective application. As a first application of the transformation equations, on a small body in the Solar system, we derived the magnitudes and colours of the minor planet 48220.

Acknowledgements

---

[10] `https://ssd.jpl.nasa.gov/horizons.cgi`

References

Bessell, M., 1990, *PASP, 102, 1181*
Bessell, M., 2005, *ARA&A, 43, 293*
Chambers, K., Magnier, E., Metcalfe, N., et al., 2016, *arXiv:1612.05560*
Flewelling, H., Magnier, E., Chambers, K., et al., 2016, *arXiv:1612.05243*
Fukugita, M., Ichikawa, T., Gunn, J., et al., 1996, *AJ, 111, 1748*
Giorgini, J., Yeomans, D., Chamberlin, A., et al., 1996, *DPS, 28, 2504*
Harris, W., 1996, *AJ, 112, 1487*
Jordi, K., Grebel, E., & Ammon, K., 2006, *A&A, 460, 339*
Kidger, M., 2003, *A&A, 408, 767*
Landolt, A., 1992, *AJ, 104, 340*
Madsen, G., & Gaensler, B., 2013, *ApJS, 209, 33*
Magnier, E., Chambers, K., Flewelling, H., et al., 2016a, *arXiv:1612.05240*
Magnier, E., Sweeney, W., Chambers, K., et al., 2016b, *arXiv:1612.05244*
Magnier, E., Schlafly, E., Finkbeiner, D., et al., 2016c, *arXiv:1612.05242*
Monet, D., Levine, S., Canzian, B., et al., 2003, *AJ, 125, 984*
Raab, H., 2012, *ascl.soft03012R*
Ramírez, I., Michel, R., Sefako, R., et al., 2012, *ApJ, 752, 5*
Stetson, P., 2000, *PASP, 112, 925*
Tonry, J., Stubbs, C., Lykke, K., et al., 2012, *ApJ, 750, 99*
Waters, C., Magnier, E., Price, P., et al., 2016, *arXiv:1612.05245*